

NON-EQUILIBRIUM DYNAMICS OF A BINARY SOLVENT AROUND HEATED  
COLLOIDAL PARTICLES

MORITZ WILKE



Bachelor Thesis

Max-Planck Institute for Intelligent Systems  
University of Stuttgart

Supervisor: Dr. Sutapa Roy  
Examiner: Priv.-Doz. Dr. Markus Bier

Thesis submitted on: August 16th, 2018



## ABSTRACT

---

Using numerical simulations, we study the non-equilibrium coarsening dynamics of a binary solvent around spherical colloids in the presence of a temperature gradient. The coarsening dynamics following a temperature quench is studied by solving the coupled modified Cahn-Hilliard-Cook equation and the heat diffusion equation, which describe the concentration profile and the temperature field, respectively. For the temperature field we apply a suitable boundary condition. We observe the formation of circular layers of different phases around the colloid whereas away from the colloid patterns of spinodal decomposition persist. Additionally, we investigate the dependence of the pattern formation on the quench temperature. Our simulation mimics an experimental system where the colloid is heated by laser illumination. Note that we look at the cooling of a solvent with an upper critical temperature, whereas the experimental analogue is the laser-heating of a solvent with a lower critical temperature. We also study a two colloid system. Here, we observe that a bridge of one phase forms connecting the two colloids. Also, we study the force acting on the colloids that is generated by the chemical potential gradient.

## ZUSAMMENFASSUNG

---

Mit Hilfe numerischer Simulationen untersuchen wir die nicht-gleichgewichtige Dynamik der Phasentrennung in Anwesenheit eines Temperaturgradienten an sphärischen kolloidalen Teilchen. Die nach einem Abschreckvorgang folgende Phasentrennung wird unter Verwendung der gekoppelten Cahn-Hilliard-Cook Gleichung und der Wärmeleitungsgleichung, die das Konzentrationsfeld und das Temperaturfeld beschreiben, untersucht. Für das Temperaturfeld benutzen wir eine passende Randbedingung. Wir beobachten, dass sich kreisförmige Schichten verschiedener Phasen um das Kolloid herum bilden, wohingegen entfernt vom Kolloid Muster erhalten bleiben, die an spinodale Entmischung erinnern. Zusätzlich untersuchen wir die Abhängigkeit der Formation der Muster von der Temperatur, auf die das Kolloid abgeschreckt wird. Unsere Simulation imitiert eine experimentelle Realisierung der Strukturbildung um in einem Lösungsmittel suspendierte Kolloide, die mit einem Laser erhitzt werden. Es ist anzumerken, dass der hier behandelte Abschreckvorgang eines Lösungsmittels mit einer oberen kritischen Temperatur einem experimentellen Erhitzen eines Lösungsmittels mit unterer kritischer Temperatur entspricht. Zusätzlich untersuchen wir ein zwei-Kolloid System. In diesem Fall formt sich eine Flüssigkeitsbrücke, die beide Kolloide miteinander verbindet. Außerdem untersuchen wir die Kraft, die aus dem Gradienten des Feldes des chemischen Potentials rührt und auf die Kolloide wirkt.



# CONTENTS

---

1	INTRODUCTION	1
2	THEORY	3
2.1	Phase separation dynamics	3
2.2	Ginzburg-Landau free energy functional	5
2.3	Cahn-Hilliard-Cook equation	6
3	MODEL AND METHOD	7
3.1	Modified Cahn-Hilliard-Cook equation and boundary conditions	7
3.2	Numerical procedure	9
4	RESULTS AND DISCUSSION	11
4.1	One colloid system	11
4.2	Two colloid system	16
4.3	Force acting on the colloids	20
5	SUMMARY AND OUTLOOK	23
A	APPENDIX	25
A.1	Non-dimensionalization of Cahn-Hilliard-Cook and heat diffusion equations	25
A.2	Non-dimensionalization of the Robin boundary condition	26
	BIBLIOGRAPHY	29



## INTRODUCTION

---

Phase separation of binary fluids is a process that everybody has seen before in their daily lives. A good example may be an oil-water mixture. At room temperature, the shaking of a salad mixture containing oil and water generates many small oil droplets getting separated out as they do not like to mix with water. Understanding the dynamics of such phase separation processes is a subject of great interest. They also hold important applications in oil and pharmaceutical industries, e.g., extraction of oil and natural gases from rocks, stability of foams, etc. John W. Cahn and John E. Hilliard devoted themselves to this non-equilibrium process of phase separation and derived in 1958 the Cahn-Hilliard equation [1]. It describes the time evolution of the local composition for spontaneous phase separation of a binary fluid.

Consider a homogeneous binary liquid mixture (A+B) above its critical temperature  $T_c$ . When we suddenly quench it below  $T_c$ , the binary liquid now lies in a non-equilibrium state and it separates into A-rich and B-rich domains which grow in size over time. The kinetics of this process is known as the *phase separation dynamics* or *coarsening*. In this thesis we consider only fluids with an upper critical temperature. That means phase separation only occurs when the temperature is below the critical temperature  $T_c$ . Coarsening processes were studied in detail for bulk systems [1]. It is of great interest to study the phase separation with effects of a surface [2] to find how phase separation processes change as compared to bulk.

We simulate a system where a single particle with a preference for one of the two components of the fluid is placed in the binary solvent. A lot of studies were devoted to understanding the phase separation phenomena in for slit geometry. It is new [3, 4] to investigate them around spherical colloidal particles. We are interested in the coarsening of a binary solvent around colloids in the presence of a time-dependent *temperature gradient*. Such systems are experimentally relevant for laser-heated colloids in a binary fluid, which have been considered in recent years [5]. It was demonstrated that when Janus particles suspended in a critical binary liquid were illuminated by light it generates a concentration gradient around the colloid [5]. This local demixing of the binary liquid at early time was hardly investigated [3, 4, 6]. This non-equilibrium dynamics is interesting and complex because of the surface effects of the particle, time-dependent temperature gradient and local phase separation.

So far, coarsening dynamics around heated colloids was studied for a single colloid only [3, 4]. In this thesis, we look at the coarsening dynamics around two colloids suspended in a near-critical binary solvent. It is not easy to guess how the presence of the second colloid will change the kinetics. This is complicated because of the temperature gradient coupled to the concentration field. The explored quantities are the time-dependent temperature field and the time-dependent order

parameter field. They are described by the modified Cahn-Hilliard-Cook equation and the heat diffusion equation. We also study the coarsening properties around a single colloid with a temperature boundary condition (b.c.) which is different from what was considered in previous works [3, 4]. Different b.c.s determine the temperature field and thus, they can control the local structure formation. We also study the forces acting on the colloid that are generated due to the gradient of the chemical potential field. For a single colloid, this force is zero and the colloid does not move. But, when two colloids are suspended in a solvent, there may be a non-zero force.

It is important to mention that we deal with a binary solvent that has an upper critical point. Therefore, to enter the two-phase state of the solvent, we must apply a temperature quench below  $T_c$ . The experimental analogue is the heating of a binary solvent with an upper critical point because it is much more practical and accessible through laser-illumination.

Rest of the thesis is structured as follows: In Sec. 2 we explain the basic theoretical backgrounds to understand the phase separation dynamics of a binary solvent and how to describe it. In Sec. 3 we derive the model of our system and mention the numerical methods we use to simulate it. Complementary, we lead through necessary calculations in the appendix (Sec. A). Section 4 presents and discusses our findings for a single colloid and a two colloid system. Lastly, Sec. 5 gives a short overview about the content of the thesis and mentions possible subsequent studies.

## THEORY

## 2.1 PHASE SEPARATION DYNAMICS

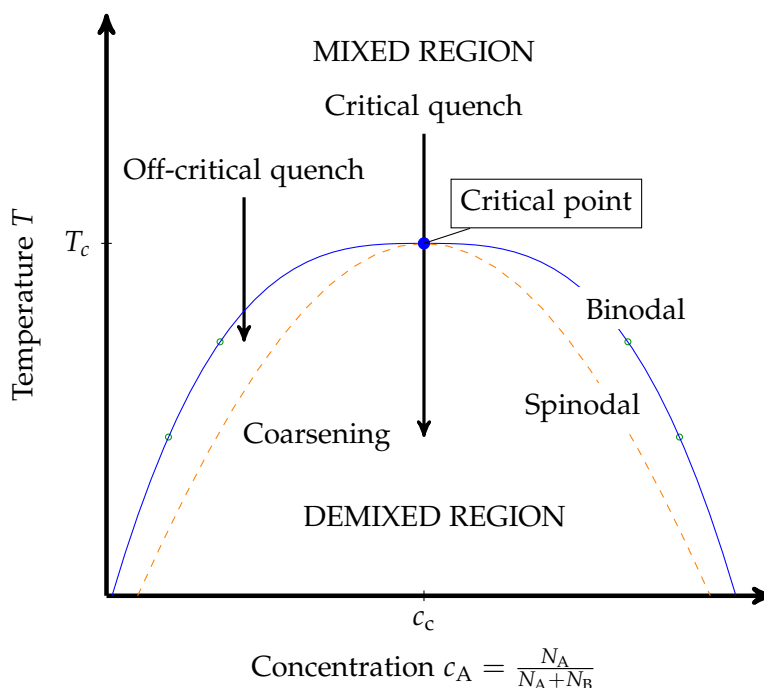


Figure 2.1: Schematic phase diagram of a binary liquid mixture with components A and B in the temperature ( $T$ ) – concentration ( $c_A$ ) plane.  $T_c$  and  $c_c$  correspond to the critical temperature and the critical concentration of the liquid, respectively. The solid blue line denotes the binodal or co-existence curve and the dashed orange line the spinodal. The left side of the binodal refers to A-rich phases, whereas the right side refers to B-rich phases. For  $T > T_c$  a liquid at critical concentration is in a homogeneously mixed state and for  $T < T_c$  it is in a demixed state. A temperature quench from a high temperature ( $> T_c$ ) to a temperature  $T < T_c$  at the critical composition leads to coarsening via spinodal decomposition (see main text for detail). On the other hand, an off-critical quench inside the region between the binodal and spinodal curves leads to coarsening via the nucleation of spherical droplets.

Phase separation is the process of unmixing of different phases of a system. Let us consider a binary liquid mixture having A and B types of particles. To explain phase separation, let us consider the phase diagram of this liquid mixture in the temperature ( $T$ ) – concentration ( $c_A$ ) plane, as shown in Fig. 2.1. Here, the concentration of species A is defined as  $c_A = N_A / (N_A + N_B)$ ;  $N_A$  is the number of particles of species A. The solid blue curve is the co-existence curve or the ‘binodal’

along which the two phases can co-exist with each other in equilibrium. Specifically, the right branch of it corresponds to the A-rich phase and the left branch to the B-rich phase.  $T_c$  and  $c_c$  are the values of the temperature and the concentration at the critical point, respectively. We will explain the broken curve later. Above  $T_c$ , the equilibrium state is the homogeneously mixed state and below  $T_c$ , it is the demixed state.

Now, when an initially homogeneous binary liquid mixture at a temperature  $T > T_c$  is suddenly quenched inside the binodal, the system falls out of equilibrium and then it moves towards the new equilibrium state which is the phase separated state with equilibrium composition values marked by green circles. However, this does not happen immediately. During the intermediate time the system goes through a complex dynamics [1] which is known as the *phase separation dynamics* or the *coarsening dynamics*. During such a process, domains of A- and B- rich phases form and they grow with time.

The ‘spinodal’ denotes the boundary between the region where the fluid will phase separate via spinodal decomposition, which is explained in the following text, and the region where the fluid is metastable. A metastable binary fluid stays in equilibrium for small concentration fluctuations but will phase separate for larger ones.

Kinetics of the phase separation process depends on the concentration of the liquid during the quench. If it is at its ‘critical’ concentration, percolating domains form [7]. This mechanism is known as the *spinodal decomposition* [1]. Typically, the average domain size,  $\ell(t)$ , during phase separation grows in a power-law with a growth exponent  $\alpha$ ,  $\ell(t) \sim t^\alpha$ . For spinodal decomposition, at early time  $\alpha = 1/3$  which corresponds to the diffusive dynamics. At very late times, the growth exponent changes. However, in this thesis we will consider the diffusive dynamics only. On the other hand, when the fluid is quenched at an ‘off-critical’ concentration inside the metastable region in between the binodal and the spinodal, phase separation occurs following *nucleation* [1] of droplets.

## 2.2 GINZBURG-LANDAU FREE ENERGY FUNCTIONAL

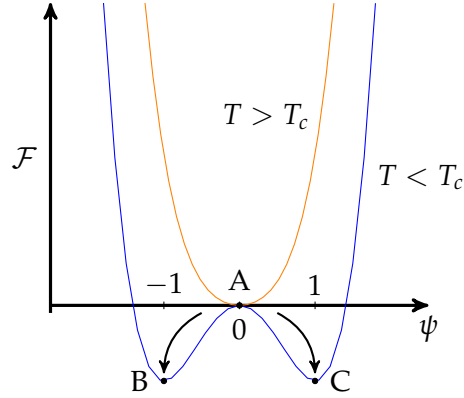


Figure 2.2: Schematic plot of the Landau free energy  $\mathcal{F}$  as a function of the order parameter  $\psi$ . The orange curve corresponds to the free energy above the critical temperature  $T_c$  with the minimum A as the equilibrium state. The blue curve corresponds to temperatures below  $T_c$  with minima B and C.

Coarsening dynamics can be understood by considering the Landau free energy whose function form is given below:

$$\mathcal{F}(\psi, T) = V \left[ \frac{a}{2} \psi^2 + \frac{u}{4} \psi^4 \right], \quad (2.1)$$

where,  $\psi$  is the order parameter we introduce as the concentration difference of the two species  $\psi = c_A - c_B$ ,  $V$  the volume,  $a$  and  $u$  are phenomenological parameters;  $a \propto (T - T_c)$ , and  $u > 0$ . For  $T > T_c$ ,  $a > 0$  and vice-versa. This free energy is schematically shown in Fig. 2.2. The equilibrium state of a system corresponds to the minimum of the free energy. It can be seen that for  $T > T_c$  there is only one minimum (point "A") at a order parameter value  $\psi = 0$  which is the fully mixed state. That means, for temperatures higher than  $T_c$  the thermodynamically favourable state of a system is the mixed state. For  $T < T_c$ , there are two minima ("B" and "C"). The system then wants to be in a phase separated state with the order parameter values given by the minima. Thus, upon a sudden temperature quench from  $T > T_c$  to a temperature inside the binodal curve, the system will fall out of equilibrium and try to move from point "A" to "B" (or "C"). However, as mentioned before, it can not move immediately. The system goes through a non-equilibrium dynamics during which domains form and grow with time.

A phase separating fluid is spatially non-uniform. To describe the behavior of a phase separating fluid, we need to allow the order parameter to be space dependent,  $\psi(\vec{r})$ . The free energy is now a functional of  $\psi(\vec{r})$  and following Ginzburg, it takes up the functional form:

$$\mathcal{F}[\psi(\vec{r}), T] = \frac{k_B T_c}{v} \int d^3 \vec{r} \left[ \frac{a}{2} \psi^2(\vec{r}) + \frac{u}{4} \psi^4(\vec{r}) + \frac{C}{2} (\nabla \psi)^2 \right]. \quad (2.2)$$

This equation is known as the *Ginzburg-Landau* free energy [8]. Here,  $C$  is a phenomenological parameter and  $v$  is an elementary volume element.

### 2.3 CAHN-HILLIARD-COOK EQUATION

During the phase separation of binary mixture (A+B), the concentration of A and B species is conserved and as a result the order parameter is also conserved. The dynamics of such a system is given by the so-called ‘Model B’ dynamics [1]. The local conservation in this case requires a continuity equation

$$\frac{\partial \psi(\vec{r}, t)}{\partial t} = -\nabla \cdot \vec{j}(\vec{r}, t), \quad (2.3)$$

where, the current,  $\vec{j}(\vec{r}, t)$ , is proportional to the gradient of the chemical potential  $\mu$  as

$$\vec{j}(\vec{r}, t) = -M\nabla\mu(\vec{r}, t). \quad (2.4)$$

$M$  is the mobility. The chemical potential  $\mu$  can be obtained as

$$\mu(\vec{r}, t) = \frac{\delta \mathcal{F}[\psi]}{\delta \psi(\vec{r}, t)}. \quad (2.5)$$

Combining Eqs. (2.3), (2.4), and (2.5), one obtains

$$\frac{\partial \psi(\vec{r}, t)}{\partial t} = M\nabla^2 \frac{\delta \mathcal{F}[\psi]}{\delta \psi(\vec{r}, t)}. \quad (2.6)$$

Insertion of the Ginzburg-Landau free energy functional of Eq. (2.2) into the above equation yields

$$\frac{\partial \psi(\vec{r}, t)}{\partial t} = \frac{Mk_B T_c}{v} \nabla^2 [a\psi(\vec{r}, t) + u\psi(\vec{r}, t)^3 - C\nabla^2\psi(\vec{r}, t)], \quad (2.7)$$

where,  $a \propto (T - T_c)$ . Equation (2.7) is known as the *Cahn-Hilliard-Cook* (CHC) equation or “model B” equation.

Note that the CHC equation in Eq. (2.7) describes a phase segregating system where the temperature is same everywhere in the system. Most of the literature is about simulating the process of coarsening after a temperature quench to a constant temperature of the whole fluid. For systems with a temperature gradient, i.e., when  $T$  depends on position  $T(\vec{r})$ , we need to modify Eq. (2.7). We will describe this later in the Sec. 3 of the thesis.

## MODEL AND METHOD

---

Our model system consists of spherical colloid (3-d) suspended in a binary solvent with an upper critical temperature  $T_c$ . Initially, the colloid and the solvent are set to a temperature  $T_0$  which is higher than the demixing critical temperature  $T_c$  of the binary solvent, so that the solvent is in a mixed phase. Next, at time  $t = 0$ , the colloid(s) is(are) quenched down to a temperature  $T_1$  below  $T_c$ . After this, a heat flow cools the solvent and a time-dependent temperature gradient is established in the system. As the solvent temperature cools below the demixing temperature  $T_c$ , the solvent starts to phase separate. We describe the non-equilibrium dynamics of the solvent after the quench with two fields: the temperature  $T(\vec{r}, t)$  and the order parameter  $\psi(\vec{r}, t)$  fields. The order parameter field is coupled to the temperature field. This coupling, together with the colloid surface effects, make the coarsening process more complex as compared to an instantaneous quench and coarsening in bulk.

### 3.1 MODIFIED CAHN-HILLIARD-COOK EQUATION AND BOUNDARY CONDITIONS

Here we explain the time evolution of  $T(\vec{r}, t)$  and  $\psi(\vec{r}, t)$ . The order parameter field is governed by the *Cahn-Hilliard-Cook* equation (described before in Sec. 2.3) for the conserved order parameter. However, the original CHC equation in Eq. (2.7) is for a system where temperature is same everywhere in the system. In order to take into account the temperature gradient present in our system we modify the equation appropriately. We replace the phenomenological parameter  $a$  by the temperature field  $\tilde{T}(\vec{r}, t) = \mathcal{A}(T(\vec{r}, t) - T_c)/T_c$  [3], where,  $\mathcal{A}$  is a positive constant. The modified CHC equation then reads

$$\frac{\partial \psi(\vec{r}, t)}{\partial t} = \frac{Mk_B T_c}{v} \nabla^2 [\tilde{T}(\vec{r}, t)\psi(\vec{r}, t) + u\psi(\vec{r}, t)^3 - C\nabla^2 \psi(\vec{r}, t)] \quad (3.1)$$

In order to consider thermal fluctuations, Gaussian white noise  $\eta(\vec{r}, t)$  is added to Eq. (3.1):

$$\begin{aligned} \frac{\partial \psi(\vec{r}, t)}{\partial t} = & \frac{Mk_B T_c}{v} \nabla^2 [\tilde{T}(\vec{r}, t)\psi(\vec{r}, t) + u\psi(\vec{r}, t)^3 - C\nabla^2 \psi(\vec{r}, t)] \\ & + \eta(\vec{r}, t). \end{aligned} \quad (3.2)$$

This Gaussian white noise has zero mean and satisfies the fluctuation-dissipation relation

$$\langle \eta(\vec{r}, t)\eta(\vec{r}', t') \rangle = -\frac{2M}{v} k_B T(\vec{r}) \nabla^2 \delta(\vec{r} - \vec{r}') \delta(t - t'). \quad (3.3)$$

Equation (3.2) is made dimensionless by scaling the dimensional variables  $r$ ,  $t$ ,  $\psi$ ,  $\eta$  by scaling factors. This calculation is shown in Sec. A.1. With the following rescaling factors (where variables without and with  $\sim$  are the dimensional and dimensionless ones, respectively), the dimensionless modified CHC equation becomes

$$\psi_0 = \left( \frac{|\tilde{T}_1|}{u} \right)^{1/2}, \quad (3.4)$$

$$r_0 = \left( \frac{C}{u\psi_0^2} \right)^{1/2} = \left( \frac{C}{|\tilde{T}_1|} \right)^{1/2}, \quad (3.5)$$

$$t_0 = \frac{\nu r_0^2}{Mk_B T_c |\tilde{T}_1|} = \frac{\nu C}{Mk_B T_c |\tilde{T}_1|^2}, \quad (3.6)$$

$$\eta_0 = \frac{\psi_0}{t_0} = \left( \frac{|\tilde{T}_1|}{u} \right)^{1/2} / \frac{\nu C}{Mk_B T_c |\tilde{T}_1|^2}, \quad (3.7)$$

$$\frac{\partial \tilde{\psi}(\tilde{\vec{r}}, \tilde{t})}{\partial \tilde{t}} = \tilde{\nabla}^2 \left[ \frac{\tilde{T}(\tilde{\vec{r}}, \tilde{t})}{\tilde{T}_1} \tilde{\psi}(\tilde{\vec{r}}, \tilde{t}) + \tilde{\psi}(\tilde{\vec{r}}, \tilde{t})^3 - \tilde{\nabla}^2 \tilde{\psi}(\tilde{\vec{r}}, \tilde{t}) \right] + \tilde{\eta}(\tilde{\vec{r}}, \tilde{t}). \quad (3.8)$$

The time evolution of the temperature field  $\tilde{T}$  is described by the **heat diffusion equation**

$$\frac{\partial \tilde{T}(\tilde{\vec{r}}, \tilde{t})}{\partial \tilde{t}} = D_{\text{th}} \tilde{\nabla}^2 \tilde{T}(\tilde{\vec{r}}, \tilde{t}), \quad (3.9)$$

whose dimensionless form is given below (for the derivation see Sec. A.1):

$$\frac{\partial \tilde{T}(\tilde{\vec{r}}, \tilde{t})}{\partial \tilde{t}} = \mathcal{D} \tilde{\nabla}^2 \tilde{T}(\tilde{\vec{r}}, \tilde{t}), \quad (3.10)$$

where,  $\mathcal{D} = D_{\text{th}} / (|\tilde{T}_1| D_m)$ ,  $D_{\text{th}}$  is the thermal diffusivity of the binary solvent and  $D_m = M(k_B T_c / \nu)$  is the interdiffusivity of the solvent at  $T_c$ .

Equation (3.10) is solved subject to boundary conditions (b.c.)

$$\tilde{T}(\tilde{\vec{r}}, \tilde{t})|_{\mathcal{C}} = \tilde{T}_1 \quad (3.11)$$

where,  $\mathcal{C}$  refers to the surface of the colloid. To maintain the temperature at the outer edges of the simulation box fixed to  $\tilde{T}_0$ , we use the following b.c.

$$\frac{\partial \tilde{T}(\tilde{\vec{r}}, \tilde{t})}{\partial \tilde{t}} = \mathcal{D} \tilde{\nabla}^2 \tilde{T}(\tilde{\vec{r}}, \tilde{t}) - c(\tilde{T}(\tilde{\vec{r}}, \tilde{t}) - \tilde{T}_0), \quad (3.12)$$

here, the sink term  $-c(\tilde{T}(\tilde{\vec{r}}, \tilde{t}) - \tilde{T}_0)$  mimics heat dissipation. We choose  $c = 0.001$  which ensures that  $\tilde{T}$  at the outer boundaries is at  $\tilde{T}_0$ .

In this thesis we consider a surface that attracts one of the two components of the fluid. To describe this preference, we consider a surface free energy term [3]

$$\mathcal{F}_S = \left[ \frac{1}{2} \alpha \int_S \psi(\tilde{\vec{r}}, \tilde{t})^2 dS - h \int_S \psi(\tilde{\vec{r}}, \tilde{t}) dS \right], \quad (3.13)$$

which we add to  $\mathcal{F}$ . Here,  $\mathcal{S}$  is the surface of the colloid,  $\alpha$  is the surface enhancement parameter and  $h$  is a symmetry-breaking surface field. The state where the free energy is lowest is the thermodynamically favorable state. That is why  $\psi$  is negative for positive  $\alpha$  and the other way around. Thus  $\alpha$  determines which phase is present near the colloid. This gives rise to an additional b.c.

$$\hat{n} \cdot \tilde{\nabla} \tilde{\psi}(\tilde{\vec{r}}, \tilde{t})|_{\mathcal{S}} = -\tilde{\alpha} \tilde{\psi}(\tilde{\vec{r}}, \tilde{t})|_{\mathcal{S}} + \tilde{h} \quad (3.14)$$

which is the so-called **Robin** boundary condition, where  $\hat{n}$  is a unit vector pointing into the colloid normal to the surface of the colloid. Here, the substitutions for non-dimensionalization are  $\alpha = (C/|\tilde{T}_1|)^{-1/2} \tilde{\alpha}$  and  $h = [|\tilde{T}_1|/(uC)^{1/2}] \tilde{h}$ , that are calculated in Sec. A.2. Another necessary boundary condition is that there is no particle flux normal to the surface of the colloid allowed:

$$(\hat{n} \cdot \nabla \mu(\vec{r}, t))|_{\mathcal{S}} = (\hat{n} \cdot \nabla \delta \mathcal{F}[\psi] / \delta \psi(\vec{r}, t))|_{\mathcal{S}} = 0. \quad (3.15)$$

### 3.2 NUMERICAL PROCEDURE

For the one-colloid system, a spherical particle of radius  $R$  is kept fixed at the center of a cubic simulation box. To start with, every simulation grid point is assigned an initial temperature value  $\tilde{T}_0 = 0.2$  and the grid points corresponding to the solvent are given an uniformly randomly generated order parameter value in the range of  $[-1, 1]$  with the condition that the spatially averaged order parameter is  $\psi_0 = 0.2$ . In Fig. 3.1, the setup is visualized for a single colloid system. At time  $t = 0$ , the colloid grid points are set to  $\tilde{T}_1 = -1$  which mimics a thermal quench. The time evolution of the system is next described by solving numerically Eqs. (3.8) and (3.10) using the Euler's method [9]. For the numerical purpose, the discrete form of the gradient and the Laplacian are used. For a function  $f(x, y, z)$  the discrete gradient is

$$\begin{aligned} \nabla f(x, y, z) \approx & [f(x+1, y, z) - f(x, y, z)] \vec{e}_x \\ & + [f(x, y+1, z) - f(x, y, z)] \vec{e}_y \\ & + [f(x, y, z+1) - f(x, y, z)] \vec{e}_z \end{aligned} \quad (3.16)$$

and the discrete Laplacian is

$$\begin{aligned} \nabla^2 f(x, y, z) \approx & f(x+1, y, z) + f(x, y+1, z) + f(x, y, z+1) \\ & + f(x-1, y, z) + f(x, y-1, z) \\ & + f(x, y, z-1) - 6 \cdot f(x, y, z). \end{aligned} \quad (3.17)$$

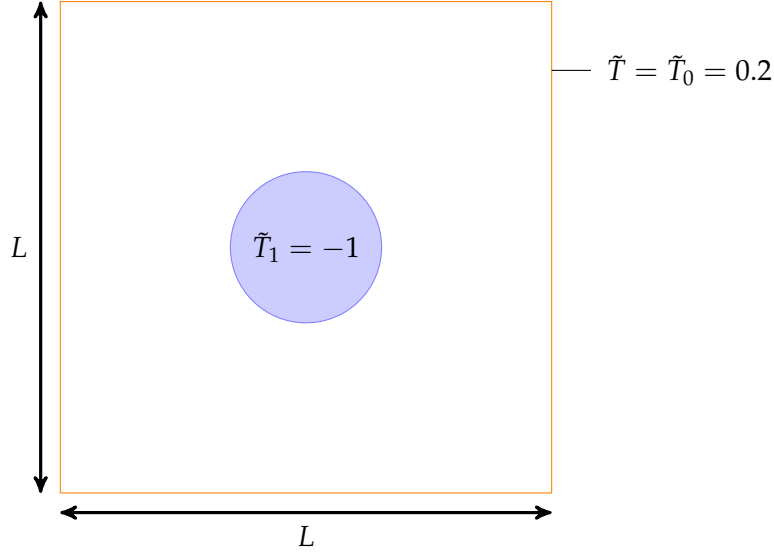


Figure 3.1: Simulation-setup of a one-colloid system in a binary solvent shown in the midplane  $(x, y)$  of the system ( $z = L/2$ ). The colloid is drawn blue and is placed in the center of the box. It is set to a quenched temperature  $\tilde{T}_1 = -1$ . Outside the colloid, each grid point is assigned an initial order parameter value from a uniformly generated random number distribution in the range  $[-1 : 1]$ , such that the mean order parameter  $\psi_0 = 0$ . Temperature at the outer edges of the simulation box are fixed to  $\tilde{T} = \tilde{T}_0 = 0.2$ .

The boundary conditions used are already mentioned before (Eqs. (3.11), (3.12), (3.14), and (3.15)). We apply **periodic boundary conditions** on the outer edges of the simulation box. This is done to avoid any surface effects on the outer edges. For lattice points  $[x(0), \dots, x(i), \dots, x(N)]$  on the  $x$  axis of a box with the length  $x(N)$  the periodic boundary conditions are applied as follows:

$$\begin{aligned} x(N+1) &= x(0) \\ x(-1) &= x(N). \end{aligned}$$

For a two colloid system, we keep two spherical particles, each of radius  $R$  in the cubic simulation box of side length  $L$ . The process of initial configuration generation is the same as for a single colloid system. At time  $t = 0$ , both colloids are quenched to temperature  $\tilde{T}_1 = -1$ . Outer edges of the simulation box are supplied with the periodic boundary condition. The b.c. for no flux in Eq. (3.15) is applied on both colloids.

All results were obtained for the parameters  $\mathcal{D} = 50$ ,  $\tilde{\alpha} = 0.5$ ,  $\tilde{h} = 1$ , and time step  $d\tilde{t} = 0.001$ . Also, all results presented in the thesis have been prepared using **Gnuplot** and **Xmgrace**.

## RESULTS AND DISCUSSION

---

Below we first present results for a single colloid system.

### 4.1 ONE COLLOID SYSTEM

We set up the simulation with a box size  $L/r_0 = \tilde{L} = 100$  and the initial conditions as in Fig. 3.1, with  $\tilde{T}_0 = 0.2$ , for a centered single colloid of radius  $R/r_0 = \tilde{R} = 10$ . Note that  $\mathcal{D} = 50$ ,  $\tilde{\alpha} = 0.5$ ,  $\tilde{h} = 1$  and  $d\tilde{t} = 0.001$ , as mentioned in the Sec. 3.2. The evolution of the system is then numerically calculated with the dimensionless heat diffusion equation (3.10) and the coupled dimensionless Cahn-Hilliard-Cook equation (3.8).

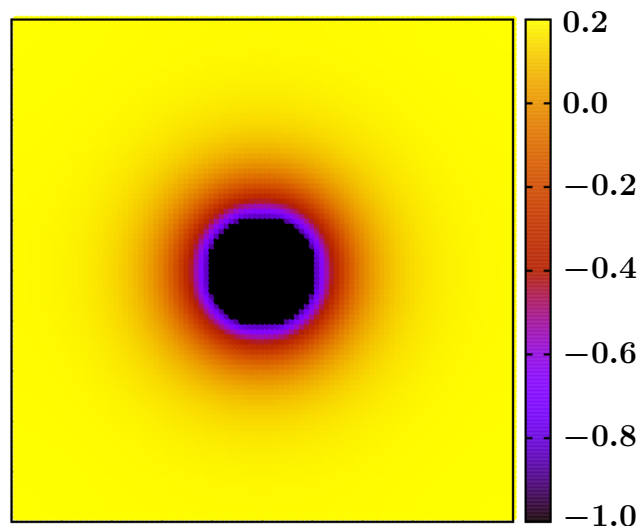


Figure 4.1: Temperature profile of the one colloid system in the midplane ( $z = L/2$ ), at an early time  $\tilde{t} = 10$ . This time is during the non-equilibrium coarsening process after a temperature quench of the colloid from an initial temperature  $\tilde{T}_0 = 0.2$  to  $\tilde{T}_1 = -1$ . Initially, the solvent was also at  $\tilde{T}_0 = 0.2$ . After a quench, the surrounding solvent gets cooled due to heat flow. The outer boundaries of the simulation box are maintained at the initial temperature 0.2 via appropriate temperature boundary condition. A large temperature gradient is established in the system.

In Fig. 4.1, we show the temperature profile in the midplane ( $z = L/2$ ) at an early time  $\tilde{t} = 10$ . The colloid is quenched to a temperature  $\tilde{T}_1 = -1$ . A large temperature gradient is present in the colloid's surrounding whereas the temperature close to the boundaries of the box is near the initial value  $\tilde{T}_0 = 0.2$ . Although this is at an

early time, the temperature field nearly has reached a steady state which is why there are no plots for different times necessary.

Figure 4.2 shows the evolution of the order parameter in the midplane of the system at six different times  $\tilde{t} = 0, \tilde{t} = 2, \tilde{t} = 10, \tilde{t} = 100, \tilde{t} = 500$  and  $\tilde{t} = 2500$ . At very early time  $\tilde{t} = 2$ , the A phase, which we call the phase with  $\tilde{\psi}(\tilde{r}, \tilde{t}) > 0$ , already accumulates around the colloid because of the colloid's preference for the component A. Away from the colloid, a pattern comparable to spinodal decomposition is present. With time, the spinodal decomposition gets more prominent (see  $\tilde{t} = 10$ ). Also as time progresses, the phases merge into circular layers around the colloid. The A phase grows around the colloid with increasing values of the order parameter surrounded by a layer of the B phase ( $\tilde{\psi}(\tilde{r}, \tilde{t}) < 0$ ). Away from the colloid a spinodal-like pattern preserves. Finally, at very late time, an almost circular very thick layer of A phase forms around the colloid (as seen at  $\tilde{t} = 2500$ ).

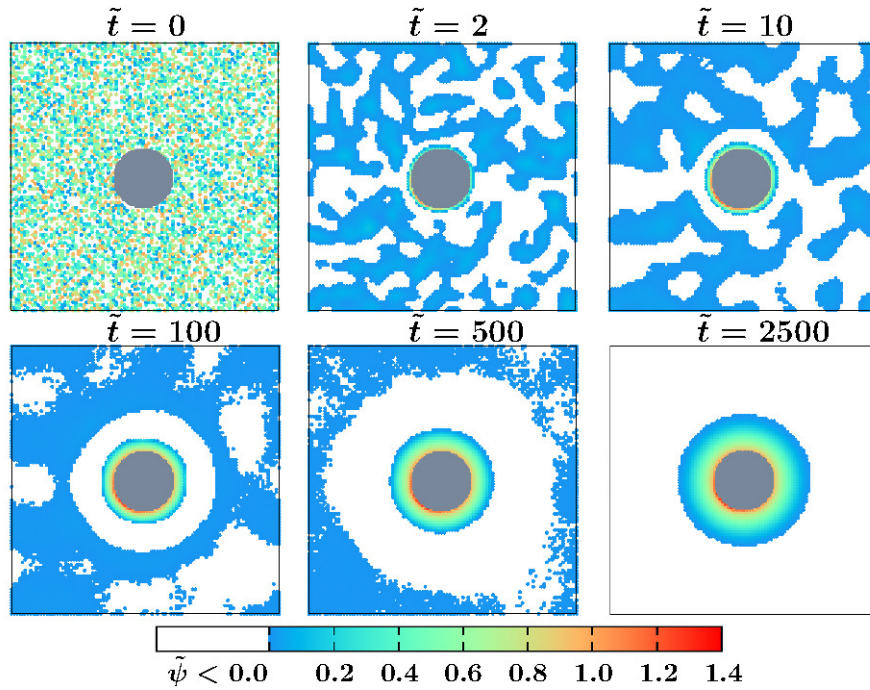


Figure 4.2: Snapshots of temperature-gradient induced coarsening of a binary solvent around a spherical colloidal particle at six different times. Results correspond to  $\tilde{L} = 100, \tilde{R} = 10, \tilde{\psi}_0 = 0, \tilde{T}_0 = 0.2$  and  $\tilde{T}_1 = -1$ . The color bar denotes the value of the order parameter. Away from the colloid spinodal-like patterns persist over time. Close to the colloid the A phase ( $\tilde{\psi}(\tilde{r}, \tilde{t}) > 0$ ) accumulates as a layer around the colloid. As time progresses, the layer broadens and a layer of the B phase ( $\tilde{\psi}(\tilde{r}, \tilde{t}) < 0$ ) forms next to it. The B phase broadens into the bulk to a large extend.

For greater insight into how the order parameter field changes over time, the angularly averaged order parameter profile  $\tilde{\psi}(\tilde{r})$  is displayed in Fig. 4.3. Positive order parameter values correspond to the A phase whereas negative values correspond to the B phase. If it is zero, it corresponds to the mixed state. For early

time  $\tilde{t} = 2$  we can already observe a layer of the A phase close to the colloid and another neighboring layer of the B phase. From  $\tilde{r} \approx 18$  onwards  $\tilde{\psi}(\tilde{r})$  stays around zero. With increasing time the maximum value of the order parameter  $\tilde{\psi}(\tilde{r}) = \tilde{R}$  on the colloid's surface increases and the A phase layer as well as the B phase layer broaden. Note that the order parameter is a conserved quantity. That means the average value is zero at any time. Consequently, the increase of the maximum value of  $\tilde{\psi}(\tilde{r})$  and the broadening of the A phase near the colloid result in a change of the B phase: The position of the minimum as well as the point from which  $\tilde{\psi}(\tilde{r})$  stays around zero shift further away from the colloid. The B phase layer broadens into the bulk which is why the absolute minimum decreases over time. The steady state order parameter profile is depicted at  $\tilde{t} = 2500$  where a very wide layer of A phase forms and the adjacent B phase order parameter has much smaller absolute value but extends over a larger radial distance such that the total order parameter is zero.

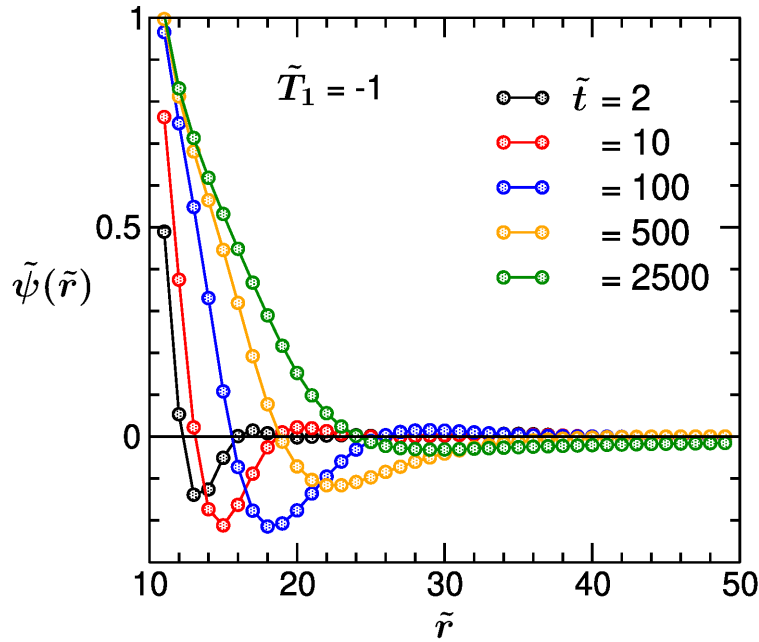


Figure 4.3: Angularly averaged order parameter (OP) profile  $\tilde{\psi}(\tilde{r})$  for the radial distance  $\tilde{r}$  with respect to the single centered colloid, at five different times  $\tilde{t}$ , starting from the colloid's surface. The A phase ( $\tilde{\psi}(\tilde{r}) > 0$ ) accumulates near the colloid surrounded by the B phase ( $\tilde{\psi}(\tilde{r}) < 0$ ). Away from the colloid,  $\tilde{\psi}(\tilde{r})$  is around zero. Over time, the A phase domain broadens near the colloid and the maximum of OP increases while the B phase domain spreads into the bulk.

In order to understand how the structure formation process gets influenced by the quench temperature, in Fig. 4.4, the evolution snapshots are presented for a deeper quench  $\tilde{T}_1 = -9$ . All other system parameters are the same as in Fig. 4.2. The qualitative nature of surface layer formation is same as for a small quench; at early time, a surface layer of phase  $\tilde{\psi} > 0$  forms and it thickens with time. In the bulk spinodal patterns coarsen. One striking difference in this case from the small

quench is that at very late time  $\tilde{t} = 100$  two layers of phase  $\tilde{\psi} > 0$  form and this second layer gets even more prominent with increasing time. For a small quench, all the way upto a time when the system reaches a stationary state, only one layer forms.

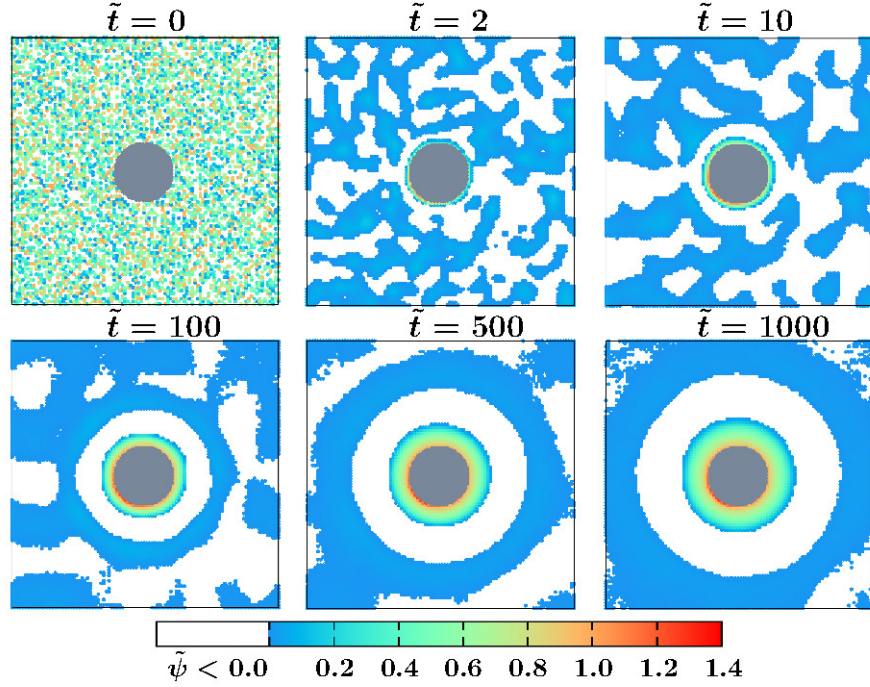


Figure 4.4: Snapshots of the binary solvent during phase separation around a quenched colloidal particle. Results correspond to a deep temperature quench at  $\tilde{T}_1 = -9$ . All other parameters are same as in Fig. 4.2. Starting from very early times, a surface layer consisting of A phase ( $\tilde{\psi}(\tilde{r}, \tilde{t}) > 0$ ) forms on the colloid's surface and spinodal-like patterns exist in the bulk. With time, a greater number of layers of A phase form, as compared to a small quench. The layered patterns also extend further away into the bulk. Note that in between two layers of A phase, a layer of B phase ( $\tilde{\psi}(\tilde{r}, \tilde{t}) < 0$ ) form.

In Fig. 4.5, the angularly averaged order parameter (OP) profile  $\tilde{\psi}(\tilde{r})$  is plotted as a function of the radial distance  $\tilde{r}$  for the deep quench to  $\tilde{T}_1 = -9$ . Qualitative features of the time evolution of the OP at early times is the same as in Fig. 4.3. However, at late times a strong difference is observed. We see that at  $\tilde{t} = 100$ , for a deep quench a second A-rich layer at  $\tilde{r} \simeq 27$  stands out as compared to a small quench  $\tilde{T}_1 = -1$ . This difference gets even stronger at a much later time  $\tilde{t} = 500$ . At this time, for a small quench the system has almost reached the steady state and only one A phase layer is seen. Whereas, for a deep quench, a very thick second A phase layer is there. To understand the physical meaning behind this, next we look at the temperature field.

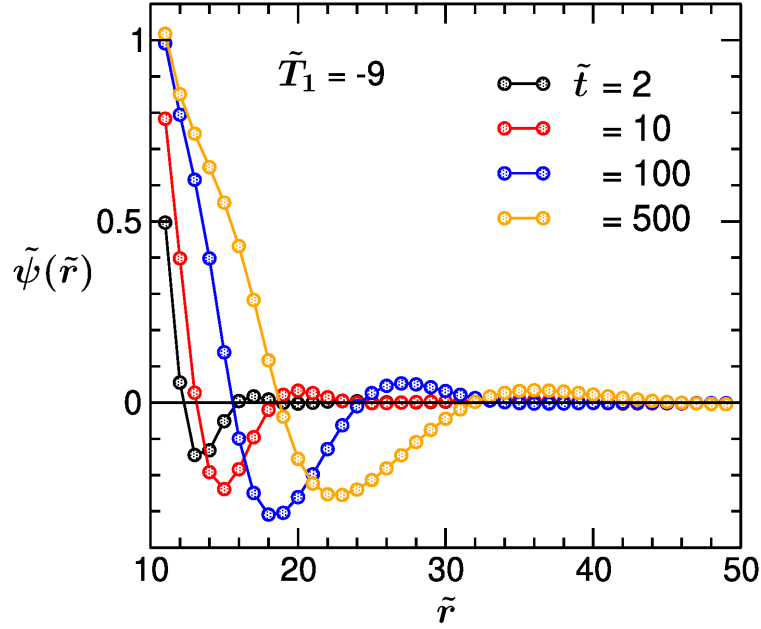


Figure 4.5: Same as Fig. 4.3, but for a deep quench  $\tilde{T}_1 = -9$ . The initial temperature is  $\tilde{T}_0 = 0.2$ . All other system parameters are same as in Fig. 4.3. Qualitatively we see the same time evolution of the order parameter  $\tilde{\psi}(\tilde{r}, \tilde{t})$  profile as for a small quench. A major difference is observed at late times: for a deep quench two prominent A phase layers are observed whereas for the small quench only one A rich layer forms. For deep quenches a greater number of rings form.

In Fig. 4.6, the angularly averaged temperature profile  $\tilde{T}(\tilde{r}, \tilde{t})$  is shown vs. the radial distance  $\tilde{r}$ , in the steady state. Results for small and deep quenches are plotted. We see that for a small quench  $\tilde{T}(\tilde{r}, \tilde{t})$  takes up negative value ( $< 0$ ) only for a smaller space region  $\tilde{r} < 20$ . But, for a deep quench,  $\tilde{T}(\tilde{r}, \tilde{t})$  is negative for a much larger distance up to  $\tilde{r} \simeq 38$ . Phase separation occurs for negative  $\tilde{T}$ , so the local phase separation for a deep quench extends for a larger spatial region and multiple rings form.

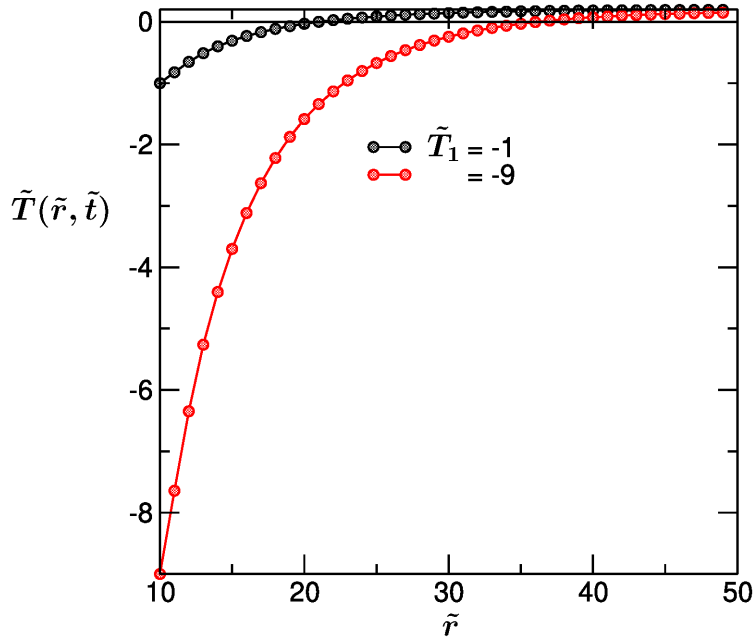


Figure 4.6: Angularly averaged temperature profile  $\tilde{T}(\tilde{r}, \tilde{t})$  vs. the radial distance  $\tilde{r}$  from the colloid center. Results correspond to a small ( $\tilde{T}_1 = -1$ ) and a deep ( $\tilde{T}_1 = -9$ ) quench. For the deep quench, the temperature field attains negative value ( $\tilde{T}(\tilde{r}) < T_c$ ) over a much larger distance from the colloid. This has an impact on the local structure formation process.

We compare the coarsening patterns that we observe in this work to the patterns in [3]. There, the layers of phases propagate through the entire simulation box, unlike the patterns observed in this thesis. This is because the stationary temperature profile in [3] is  $\tilde{T}_1 = -1$  everywhere in the system. So, the solvent phase separates globally. On the other hand, for the b.c. used in this thesis, a temperature gradient always exists in the system, with the temperature value on the surface of the colloid and at the outer edges of the simulation box being  $\tilde{T}_1$  and  $\tilde{T}_0$ , respectively. This leads to a local phase separation and less number of rings form.

#### 4.2 TWO COLLOID SYSTEM

We present results for the two-colloid system. In this case, two identical spherical colloids are kept fixed in the binary solvent. The system is initially at a temperature above  $T_c$  and at time  $\tilde{t} = 0$ , both colloids are quenched to a temperature  $\tilde{T}_1$  below  $T_c$  and have same surface properties. Both colloids are equally far away from the center of the simulation box and lie in the middle of the  $y$ - and  $z$ -axis. We apply the same numerical procedure as before.

In Fig. 4.7, we show the temperature profile in the midplane of the system  $z = L/2$ , at an early time  $\tilde{t} = 2$ . System sizes and colloid radius that we choose are  $\tilde{L} = 80$ ,  $\tilde{R} = 5$  and the surface parameters are  $\tilde{\alpha} = 0.5$ ,  $\tilde{h} = 1$ . The color bar shows different values of the temperature. Both colloids are at temperature  $-1$ , marked by the black color. Near both colloids' surfaces a large temperature gradient is visible,

while close to the outer edges of the simulation box values of  $\tilde{T}(\vec{r})$  are close to the initial temperature  $\tilde{T}_1$ . Note that outer edges are maintained at  $\tilde{T}_0 = 0.2$  via suitable b.c. The purple region corresponding to a low temperature ( $\tilde{T}(\vec{r}, t) \approx -0.75$ ) forms a temperature bridge connecting both colloids. Thus, the temperature fields of the two colloids get coupled. This kind of coupling should have immediate influence in the order parameter field as well.

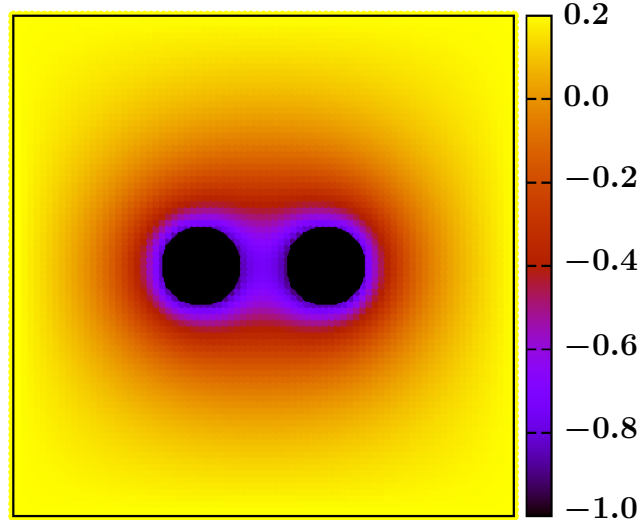


Figure 4.7: Temperature profile of the two colloid system at an early time  $\tilde{t} = 2$  in the midplane ( $z = L/2$ ) of the system. Both colloids are quenched to a temperature  $\tilde{T}_1 = -1$  and the initial temperature is  $\tilde{T}_0 = 0.2$ . The temperature at the outer boundaries of the box is kept fixed at  $\tilde{T}_0 = 0.2$ . A large temperature gradient is established and the temperature fields of the two colloids get coupled with each other.

Next, in Fig. 4.8, we present the coarsening snapshots in the midplane of the system  $z = L/2$  at different times. The system parameters are chosen to be  $\tilde{L} = 120$ ,  $\tilde{R} = 10$ ,  $\tilde{\psi}_0 = 0$ ,  $\tilde{T}_0 = 0.2$  and  $\tilde{T}_1 = -1$ . At early time, the evolution around each colloid is qualitatively similar to what we saw for the single colloid. On each colloid a surface layer with A phase ( $\tilde{\psi} > 0$ ) forms and spinodal-like patterns exist away from the colloids. With time, these layers get thicker and the value of the order parameter on the surface layer increases (clear from different colors in the figure), while their shape stays circular. At the same time, the spinodal domains also get bigger. At very late time ( $\tilde{t} = 800$ ), the surface layers of each colloid touch each other, they get coupled and a bridge forms. This liquid bridge is ‘dumbbell’-shaped. With further time, this bridge will evolve. But we do not present results from later times because the simulations are expensive.

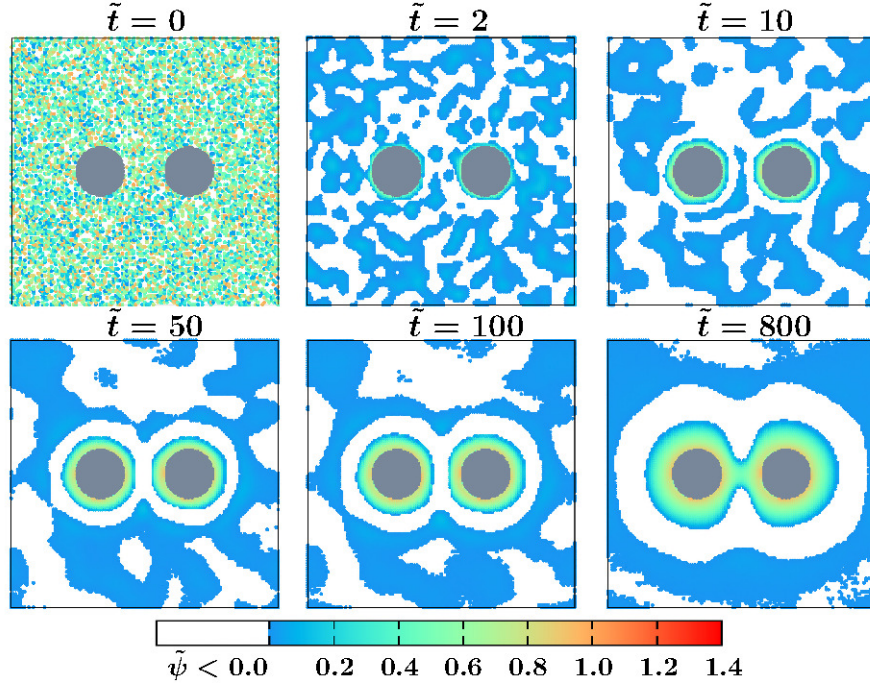


Figure 4.8: Snapshots of temperature-gradient induced coarsening of a binary solvent around two spherical colloidal particles at six different times. Results correspond to  $\tilde{L} = 120$ ,  $\tilde{R} = 10$ ,  $\tilde{\psi}_0 = 0$ ,  $\tilde{T}_0 = 0.2$  and  $\tilde{T}_1 = -1$ . At early time the A phase accumulates around each colloid. At  $\tilde{t} = 20$  the inner A phase layers of both colloid merge resulting in a coupled layer formation. In the bulk a spinodal-like pattern persists over time.

We find that the time  $\tilde{t}_0$  at which two individual layers (for each colloid) merge depend on the separation distance  $\tilde{d}$  between the two colloids. In Fig. 4.9, this is shown for various values of  $\tilde{d}$ . The symbol there corresponds to simulation data and the dashed curve a guide to the eye.

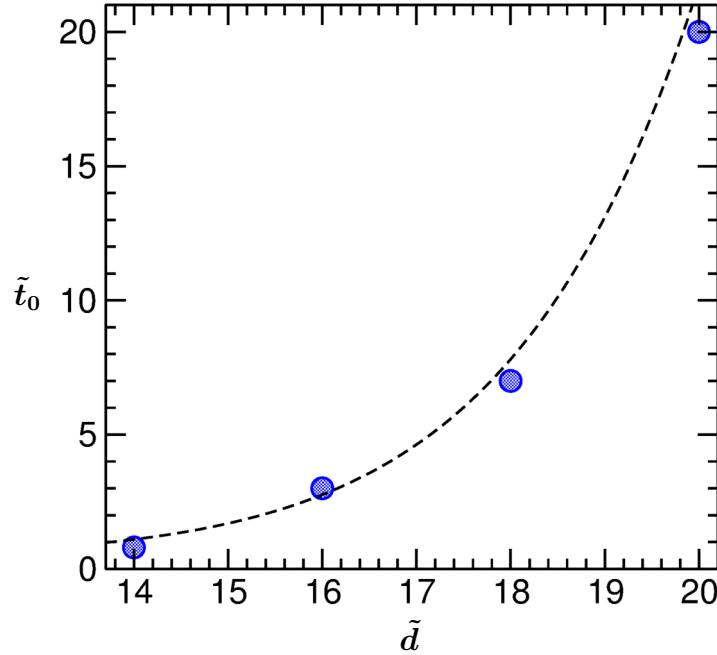


Figure 4.9: Plot of the time  $\tilde{t}_0$  at which the individual surface layers for two colloids merge with each other vs. the separation distance  $\tilde{d}$  between the two colloids. The dashed curve is a guide to the eye.

In Fig. 4.10, the order parameter (OP) value  $\tilde{\psi}(\tilde{x}, \tilde{t})$  is plotted as a function of the  $x$ -coordinate, along the  $x$ -axis in the midplane  $z = L/2$  of the system. In this case,  $\tilde{L} = 120$ ,  $\tilde{R} = 10$  and the two colloids are placed at  $(40, 60, 60)$  and  $(80, 60, 60)$ , respectively. The OP in the region in between the two colloids is presented in Fig. 4.10. Note that  $\tilde{x} = 50$  and  $\tilde{x} = 70$  denote the surface of the colloids. At very early time  $\tilde{t} = 2$ , a surface layer of the phase  $\tilde{\psi} > 0$ , followed by a depletion layer of  $\tilde{\psi} < 0$  form on both colloids, as visible in the figure. In the middle the OP stays close to zero. With increasing time, thickness of these surface layers as well as the depletion layers increase and the region with zero OP almost vanishes. At time  $\tilde{t} = 50$  onwards, the two depletion layers have merged and only one sinusoidal layer of phase  $\tilde{\psi} < 0$  exists in between the two colloids. The surface layers have also increased in thickness. Finally, at very late time  $\tilde{t} = 800$ , the OP value in the whole region in between the two colloids has become positive. This corresponds to a physical situation in which a liquid bridge of phase  $\tilde{\psi} > 0$  has formed covering both colloids. This total OP in the system, however, stays zero which is clear from the snapshots in Fig. 4.8. Note that the profiles in Fig. 4.10 will be symmetric with respect to both colloids upon averaging over multiple initial configurations. Here we present them only from a single realization.

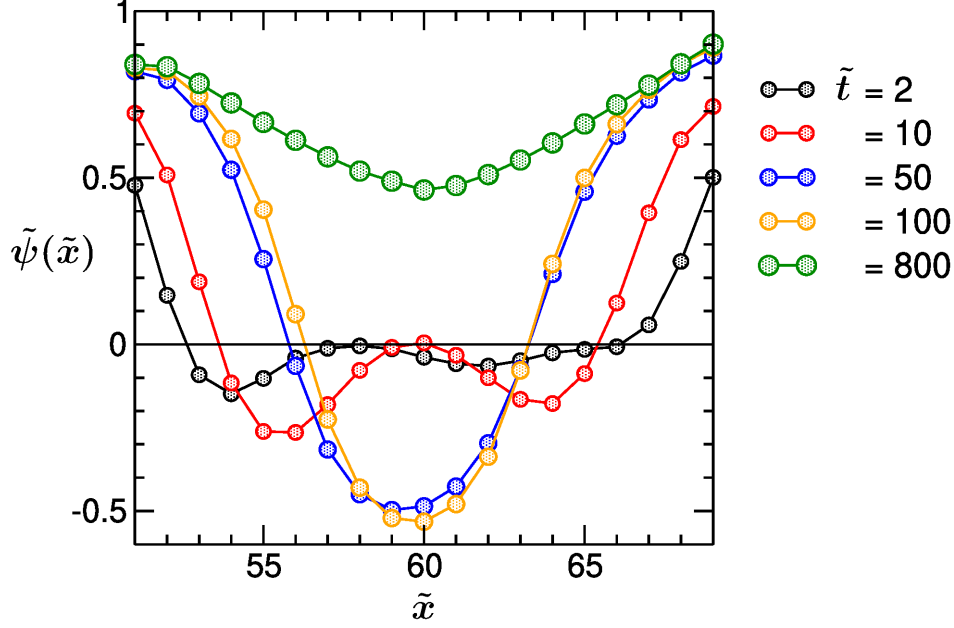


Figure 4.10: Plot of the order parameter (OP) as a function of the  $x$ -coordinate in between two colloids. Results correspond to  $\tilde{L} = 120$ ,  $\tilde{R} = 10$ ,  $\tilde{T}_0 = 0.2$ ,  $\tilde{T}_1 = -1$ ,  $\tilde{\alpha} = 0.5$ , and  $\tilde{h} = 1$ .  $\tilde{x} = 50$  and  $\tilde{x} = 70$  depict two colloid surfaces and the space in between corresponds to the solvent. The OP value along the  $x$ -axis in the midplane of the system is presented. A layer of phase  $\tilde{\psi} > 0$  and a neighboring depletion layer of  $\tilde{\psi} < 0$  form near each colloid whereas  $\tilde{\psi} \approx 0$  in the middle. Over time the layers broaden and the maximum value of OP on the colloid surfaces increases. At  $\tilde{t} = 50$  the depletion layers have merged so that one sinusoidal layer of  $\tilde{\psi} < 0$  exists in the middle. At late time  $\tilde{t} = 800$  the layers of phase  $\tilde{\psi} > 0$  have broadened over the whole region, displaced the other layer and merged into one covering both colloids.

#### 4.3 FORCE ACTING ON THE COLLOIDS

We also investigate the forces acting on two suspended colloidal particles in a near-critical solvent. This force arises due to the gradient of the chemical potential of the solvent. During the non-equilibrium coarsening processes, the temperature field and the coupled order parameter field change with time. As a result, the chemical potential field also changes with time. The generalized force  $\tilde{F}$ , which we are interested in, is proportional to  $\tilde{\psi}(\tilde{r}, \tilde{t}) \nabla \tilde{\mu}(\tilde{r}, \tilde{t})$ . The net force acting on a colloid is given by the integral over the colloid surface. For a single colloid, this force  $\tilde{F}$  is expected to be zero and the colloid does not move. However, when there are two colloids in the solvent very close to each other (i.e., the separation distance is small enough) a non-zero force may act on each colloid.

In Fig. 4.11, we plot the  $x$ -coordinate of the averaged force  $\tilde{F}$  as a function of time  $\tilde{t}$  following a temperature quench of both colloids from an initial temperature  $\tilde{T}_0 = 0.2$  to  $\tilde{T}_1 = -1$ . The system size and the colloid radius considered are  $\tilde{L}_x = 140$ ,  $\tilde{L}_y = \tilde{L}_z = 50$ ,  $\tilde{R} = 5$ . The first and second colloids are kept at locations  $(65, 25, 25)$ ,  $(85, 25, 25)$ , respectively. That means we have a center to center separation distance

$\tilde{d} = 20$ . The data is averaged over 5 independent initial conditions. The black data corresponds to the force acting on the single colloid.  $\mathcal{D}$  is taken to be 100. Here, we plot only the force acting on the first colloid. As a reference, the force acting on a single colloid is also presented in this plot. For the single colloid we take  $\tilde{L}_x = 100$ ,  $\tilde{L}_y = \tilde{L}_z = 50$ ,  $\tilde{R} = 5$  and the colloid is placed fixed at the center of the box. All other parameters for the single colloid case are the same as for the two-colloid case. First of all, following a very early-time window, the average force  $\tilde{F}$  for a single colloid saturates to zero very quickly, i.e., the colloid can not move. For the two-colloid case, following a temperature quench the colloid experiences a non-zero force  $\tilde{F}$  which initially increases with increasing time, then it reaches a certain threshold and after that it starts decaying and at very late time finally saturates to zero. The time when this force decays to zero depends on the separation distance  $\tilde{d}$ . It decays faster for smaller  $\tilde{d}$ . The maximum value of the force  $\tilde{F}$  is also larger for smaller  $\tilde{d}$ .

Since this force  $\tilde{F}$  appears only upon confinement, let us denote the time-dependent force acting on colloid 1 for the two-colloid system as  $\tilde{F}_{\text{two}}(\tilde{t})$  and the force acting on a single colloid as  $\tilde{F}_{\text{single}}$ . One can then write,  $\tilde{F}_{\text{two}}(\tilde{t}) = \tilde{F}_{\text{single}} + \tilde{F}_{\text{excess}}$ . As clear from Fig. 4.11, this excess force  $\tilde{F}_{\text{excess}}$  starts from zero and decays to zero at very late time. In the intermediate time this is non-monotonic. In future, we will do a scaling analysis of this excess force  $\tilde{F}_{\text{excess}}$ .

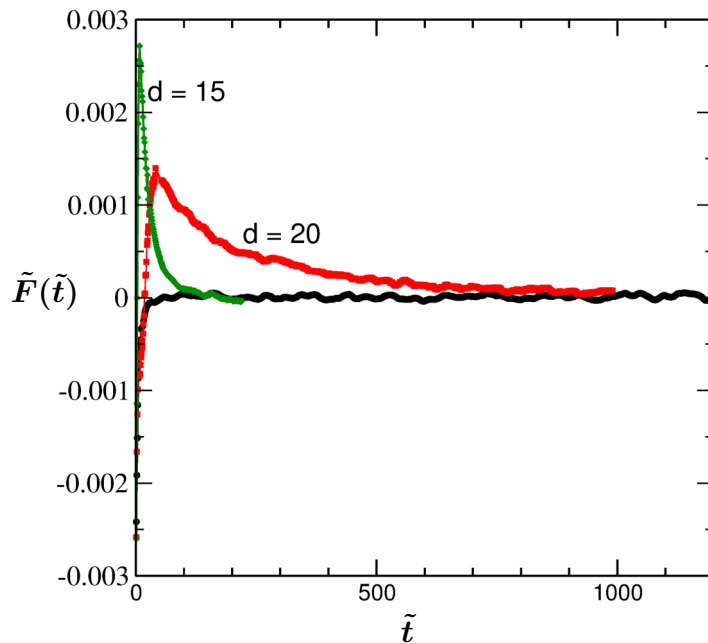


Figure 4.11: Plot of the force  $\tilde{F}(\tilde{t})$  acting on one of the two colloids during coarsening, resulting from a chemical potential gradient as a function of time  $\tilde{t}$ . See main text for the definition of  $\tilde{F}(\tilde{t})$ . The maximum value of  $\tilde{F}(\tilde{t})$  is larger for shorter separation distances.



## SUMMARY AND OUTLOOK

We have presented results for the numerical simulation of the non-equilibrium dynamics of the temperature-gradient induced coarsening of a binary solvent around spherical colloidal particles at its critical concentration. Initially, the colloid as well as the solvent are set to temperature  $\tilde{T}_0$  above the critical temperature of the solvent. Then, the colloid is quenched to a temperature  $\tilde{T}_1$  below the critical temperature, establishing a temperature gradient in the system. The temperature gradient is maintained by suitable boundary condition (b.c.). The outer boundaries of the simulation box are always at the initial temperature  $\tilde{T}_0$  and the colloid is always at the quench temperature  $\tilde{T}_1$ . We use a b.c. that is different from the ones used in earlier works [3, 4]. We simulated an one colloid system as well as a two colloid system and incorporated the colloid's adsorption preference by applying the **Robin** boundary condition. The observed quantities are the time-dependent temperature field and the time-dependent order parameter field which are described by the modified Cahn-Hilliard-Cook equation coupled with the heat diffusion equation.

We found that circular layers of phase A and phase B, referring to the components of the solvent, form around the colloid. Two neighboring layers are of opposite phase. Away from the surface, spinodal-like patterns exist. The layers near the colloid evolve and broaden into the bulk while increasing their respective concentration ( $c_A$  for phase A and  $c_B$  for phase B) over time. By simulating the two colloid system we observed the coupling of the layer formation of each colloid. At very early time one layer forms close to each colloid separately. As time progresses, these layers merge into a 'dumbbell'-shaped liquid bridge which connects both colloids. For deep quenches we observed the formation of a greater number of layers. We also studied the force acting on suspended colloids due to the gradient in the chemical potential field close to the surface. The force acting on a single colloid is zero which means the colloid does not move. For two colloids suspended in the near-critical solvent, for short separation distances, a non-zero force acts on each colloid. This force increases in magnitude with decreasing separation distance.

In our model, we assumed the mobility  $M$  and the thermal diffusivity  $D_{th}$  to be constant; although in reality they depend on  $\psi$ . This leaves space for an improvement in future works. The results in this thesis are obtained for colloids in the bulk. It is certainly interesting to simulate our system also in confinement and calculate the force acting on the colloids in confinement. In general, our model offers a lot of possibilities for simulations to investigate influences on the coarsening patterns and temperature profile. It is possible to simulate more colloids in one system, change their adsorption preferences and their positioning. Also, Janus particles can be used where the two hemispheres of the particle have different

temperature and different surface properties. Additionally, temperature quenches can be activated in a sinusoidal way.

## APPENDIX

---

### A.1 NON-DIMENSIONALIZATION OF CAHN-HILLIARD-COOK AND HEAT DIFFUSION EQUATIONS

In order to convert the dimensional equations Eqs. (3.2) and (3.9) to corresponding dimensionless forms, let us apply the substitutions  $\vec{r} = \tilde{r}\tilde{r}_0$ ,  $t = \tilde{t}t_0$ ,  $\psi(\vec{r}, t) = \tilde{\psi}(\tilde{r}, \tilde{t})\psi_0$ , and  $\eta(\vec{r}, t) = \tilde{\eta}(\tilde{r}, \tilde{t})\eta_0$ . The quantities with index 0 are the rescaling coefficients and the symbol  $\sim$  above the quantities refers to the quantities without dimension.

As a preparation, the derivative with respect to t and the derivative with respect to r are converted as:

$$\frac{\partial}{\partial r} = \frac{\partial}{\partial \tilde{r}} \frac{\partial \tilde{r}}{\partial r} = \frac{1}{r_0} \frac{\partial}{\partial \tilde{r}'} \quad (\text{A.1})$$

$$\frac{\partial}{\partial t} = \frac{1}{t_0} \frac{\partial}{\partial \tilde{t}}. \quad (\text{A.2})$$

For the sake of completeness, let us recall here again the dimensional form of the CHC equation in Eq. (3.2)

$$\begin{aligned} \frac{\partial \psi(\vec{r}, t)}{\partial t} = & \frac{Mk_B T_c}{v} \nabla^2 [\tilde{T}(\vec{r}, t)\psi(\vec{r}, t) + u\psi(\vec{r}, t)^3 \\ & - C\nabla^2 \psi(\vec{r}, t)] + \eta(\vec{r}, t) \end{aligned} \quad (\text{A.3})$$

Inserting the above-mentioned substitutions and the converted derivations in Eq. (A.3) yields

$$\begin{aligned} \frac{\partial \tilde{\psi}(\tilde{r}, \tilde{t})}{\partial \tilde{t}} = & \frac{Mk_B T_c}{v} \frac{t_0}{r_0^2} \tilde{\nabla}^2 [\tilde{T}(\tilde{r}, \tilde{t})\tilde{\psi}(\tilde{r}, \tilde{t}) + u\psi_0^2 \tilde{\psi}(\tilde{r}, \tilde{t})^3 \\ & - \frac{C}{r_0^2} (\tilde{\nabla}^2 \tilde{\psi}(\tilde{r}, \tilde{t}))] + \frac{t_0}{\psi_0} \eta_0 \tilde{\eta}(\tilde{r}, \tilde{t}). \end{aligned} \quad (\text{A.4})$$

Analogously this is done for the heat diffusion equation (3.9):

$$\frac{\partial \tilde{T}(\tilde{r}, \tilde{t})}{\partial \tilde{t}} = D_{\text{th}} \frac{t_0}{r_0^2} \tilde{\nabla}^2 \tilde{T}(\tilde{r}, \tilde{t}). \quad (\text{A.5})$$

For equation (A.4) to be dimensionless the rescaling coefficients can be chosen such that the following is satisfied:

$$\frac{Mk_B T_c t_0 |\tilde{T}_1|}{v r_0^2} = \frac{Mk_B T_c t_0 u \psi_0^2}{v r_0^2} = \frac{Mk_B T_c t_0 C}{v r_0^4} = \frac{t_0 \eta_0}{\psi_0} = 1. \quad (\text{A.6})$$

As a result one obtains the following rescaling factors:

$$\psi_0 = \left( \frac{|\tilde{T}_1|}{u} \right)^{1/2}, \quad (\text{A.7})$$

$$r_0 = \left( \frac{C}{u\psi_0^2} \right)^{1/2} = \left( \frac{C}{|\tilde{T}_1|} \right)^{1/2} \quad (\text{A.8})$$

$$t_0 = \frac{\nu r_0^2}{Mk_B T_c |\tilde{T}_1|} = \frac{\nu C}{Mk_B T_c |\tilde{T}_1|^2} \text{ and} \quad (\text{A.9})$$

$$\eta_0 = \frac{\psi_0}{t_0} = \left( \frac{|\tilde{T}_1|}{u} \right)^{1/2} / \frac{\nu C}{Mk_B T_c |\tilde{T}_1|^2}. \quad (\text{A.10})$$

Using these factors in Eq. (A.5) leads to

$$\frac{\partial \tilde{T}(\tilde{\vec{r}}, \tilde{t})}{\partial \tilde{t}} = D_{\text{th}} \frac{\nu}{Mk_B T_c |\tilde{T}_1|} \tilde{\nabla}^2 \tilde{T}(\tilde{\vec{r}}, \tilde{t}) \quad (\text{A.11})$$

$$= \frac{D_{\text{th}}}{D_m |\tilde{T}_1|} \tilde{\nabla}^2 \tilde{T}(\tilde{\vec{r}}, \tilde{t}) \quad (\text{A.12})$$

$$= \mathcal{D} \tilde{\nabla}^2 \tilde{T}(\tilde{\vec{r}}, \tilde{t}) \quad (\text{A.13})$$

where  $D_m(T_c) = Mk_B T_c / \nu$  is the interdiffusion constant of the binary solvent at temperature  $T_c$  and  $\mathcal{D} = D_{\text{th}} / (D_m |\tilde{T}_1|)$ .

## A.2 NON-DIMENSIONALIZATION OF THE ROBIN BOUNDARY CONDITION

For converting the Robin boundary condition

$$h = \left[ \hat{n} \cdot \nabla \psi(\vec{r}, t) + \alpha \psi(\vec{r}, t) \right] \Big|_{\mathcal{S}} \quad (\text{A.14})$$

to a dimensionless equation, the substitutions  $\alpha = \tilde{\alpha} \alpha_0$ ,  $\psi(\vec{r}, t) = \tilde{\psi}(\tilde{\vec{r}}, \tilde{t}) \psi_0$ ,  $\vec{r} = \tilde{\vec{r}} r_0$  and  $h = \tilde{h} h_0$  are used.

Inserting the substitutions in Eq. (A.14) and using Eq. (A.1), one obtains

$$\tilde{h} h_0 = \left[ \frac{\psi_0}{r_0} \frac{\partial \tilde{\psi}(\tilde{\vec{r}}, \tilde{t})}{\partial \tilde{r}} + \alpha_0 \psi_0 \tilde{\alpha} \tilde{\psi}(\tilde{\vec{r}}, \tilde{t}) \right] \Big|_{\mathcal{S}}. \quad (\text{A.15})$$

For Eq. (A.15) to be dimensionless the rescaling coefficients are chosen analogously to Sec. A.1 so that

$$\frac{\psi_0}{r_0 h_0} = \frac{\alpha_0 \psi_0}{h_0} = 1. \quad (\text{A.16})$$

As a result one obtains the following rescaling factors:

$$\alpha_0 = \frac{1}{r_0} \stackrel{\text{(A.8)}}{=} \left( \frac{|\tilde{T}_1|}{C} \right)^{1/2} \quad (\text{A.17})$$

$$h_0 = \frac{\psi_0}{r_0} \stackrel{\text{(A.7)}}{\stackrel{\text{(A.8)}}{=}} \frac{|\tilde{T}_1|}{(uC)^{1/2}}. \quad (\text{A.18})$$



## BIBLIOGRAPHY

---

- [1] K. Binder, in *Kinetics of Phase Transitions*, edited by S. Puri, and V. Wadhawan, (CRC, Boca Raton, FL, 2009), p.62.
- [2] S. K. Das, S. Puri, J. Horbach, and K. Binder, *Phys. Rev. Lett.* **96**, 016107 (2006).
- [3] S. Roy, S. Dietrich, and A. Maciolek, *Phys. Rev. E* **97**, 042603 (2018).
- [4] S. Roy, and A. Maciolek, arXiv 1806.08623 (2018).
- [5] I. Buttinoni, G. Volpe, F. Kummel, G. Volpe, and C. Bechinger, *J. Phys.: Condens. Matter* **24**, 284129 (2012).
- [6] J. R. Gomez-Solano, S. Roy, A. Maciolek, and S. Dietrich, to be published, (2018).
- [7] S. Roy and S. K. Das, *J. Chem. Phys.* **139**, 044911 (2013).
- [8] P. C. Hohenberg and A. P. Krekhov, *Physics Reports* **572**, 0370 (2015).
- [9] M.P. Allen and D.J. Tildesley, *Computer Simulations of Liquids*, (Clarendon, Oxford, 1987).



## DECLARATION

---

Ich erkläre hiermit,

- dass ich diese Bachelorarbeit selbständig verfasst habe,
- dass ich keine anderen als die angegebenen Quellen verwendet und alle wörtlich oder sinngemäß aus anderen Werken übernommenen Aussagen als solche gekennzeichnet habe,
- dass die eingereichte Arbeit weder vollständig noch in wesentlichen Teilen Gegenstand eines anderen Prüfungsverfahrens ist,
- dass ich die Arbeit weder vollständig noch in Teilen bereits veröffentlicht habe
- und dass der Inhalt des elektronischen Exemplares mit dem des Druckexemplares übereinstimmt.

*Stuttgart, August 16th, 2018*

---

Moritz Wilke



#### COLOPHON

This document was typeset using the typographical look-and-feel classicthesis developed by André Miede and Ivo Pletikosić. The style was inspired by Robert Bringhurst's seminal book on typography "*The Elements of Typographic Style*".